Advances in Colloid and Interface Science 247 (2017) 163–171

Contents lists available at ScienceDirect

Advances in Colloid and Interface Science

journal homepage: www.elsevier.com/locate/cis

Historical Perspective

# Interfacial characteristics of binary polymer blend films spread at the air-water interface

Masami Kawaguchi

*Laboratory of Colloid Rheology, Division of Chemistry for Materials, Graduate School of Engineering, Mie University, 1577 Kurimamachiya, Tsu, Mie 514-8507, Japan*

ARTICLE INFO

*Keywords:*
Binary polymer blend films
Air-water interface
Miscibility
Surface pressure
Structural properties
Dilational moduli

ABSTRACT

The interfacial characteristics of binary polymer blend films spread at the air-water interface are reviewed, focusing on their surface pressures, interfacial structures, and dilational moduli as a function of the miscibility. Miscible polymer blend films show thermodynamic, structural, and dynamic properties which are a combination of those from both components in the polymer blend present at the air-water interface. No preferential adsorption is observed and the behavior does not depend on the surface concentration regime. In contrast, for immiscible polymer blend films, preferential adsorption of one polymer phase occurs at the air-water interface and the interfacial characteristics in the semi-dilute and concentrated regimes are strongly controlled by one of the components of the adsorbed polymer.

## 1. Introduction

Binary polymer blend films spread at the air-water interface are of much interest for e.g. biological systems, membranes, foams, food processing, and cosmetics. Such a system can also provide important information about the thermodynamic interactions, structural orientation and packing, and dynamic dilational properties of the blended polymers. Polymer blend films are generally formed by two water-insoluble polymers and by a water-insoluble polymer and a water-soluble polymer, irrespective of their miscibility. Thus, clear difference between the corresponding polymer blend films should be observed in their interfacial properties, such as surface pressures, structural properties, and dilational moduli by plotting them as a function of total surface concentration in the polymer blends. However, the most important open physical problems have not been well understood yet in quasi-two dimensional polymer blend systems.

Commonly, in the thermodynamic studies of binary polymer blend films spread at the air-water interface, an understanding of their miscibility is one of the most important factors. The miscibility can be determined by fitting a plot of the mean surface area ($A$) measured at a fixed surface pressure as a function of the composition of one polymer in the blend, where the "additive line" is defined by Eq. (1).

$$A_{12} = A_1X_1 + A_2X_2 \tag{1}$$

where $A_{12}$ is the mean surface area, $A_1$ and $A_2$ are the surface areas of polymer 1 and 2, respectively, and $X_1$ and $X_2$ are the molar fraction of the corresponding polymer films. A binary polymer blend is considered an ideal or completely immiscible mixture when the plot matches the additive line. Negative and positive deviations from the additive line correspond to miscible and immiscible binary polymer blend films, respectively. Such deviations are attributed to the intermolecular interactions between the repeating monomeric units of the polymer blends, such as hydrogen bonding, hydrophobic bonding, and steric interactions [1]. The two polymer components in miscible polymer blend films often have the same interfacial orientation at the air-water interface, whereas immiscible films they have different orientations [1–3].

Analysis of the structural properties of binary polymer blend films spread at the air-water interface should provide their interfacial orientations and changes in the conformation of the individual polymer chains at the air-water interface in the presence of other polymer chains. Since optical reflection methods and neutron reflectivity techniques have been applied to polymer films spread at the air-water interface [1,3,4], such methods could be powerful techniques for obtaining the structural properties of binary polymer blend films. Moreover, atomic force microscopy (AFM) techniques provide some morphological information of the binary polymer blend films after the films first need to be deposited on a solid surface using the Langmuir-Blodgett (LB) technique [4].

Dynamic dilational properties of the binary polymer blend films spread at the air-water interface strongly depend on relaxation processes such as polymer chain reorientation and chain conformation by variations in the surface area [5]. The dynamic dilational moduli are often measured by oscillations of barriers in Langmuir troughs and capillary wave methods that detect surface light scattering and excited wave techniques. In most oscillatory barrier measurements, the

*E-mail address:* kawaguti@chem.mie-u.ac.jp.

http://dx.doi.org/10.1016/j.cis.2017.05.004
Received 22 December 2016
Available online 04 May 2017
0001-8686/ 

amplitudes of the surface deformation strains are < 10% and the frequencies are below 1 Hz. For the determinations of dynamic dilational moduli, it is necessary to know whether the stress-strain plot is linear or non-linear due to somewhat large strain. On the other hand, the surface light scattering and excited wave methods apply very small deformation strains (< $10^{-3}$%) at high frequencies (> 100 Hz).

In most previous work on binary polymer blend films spread at the air-water interface, the miscibility was one of the most studied issues and the interesting results of their thermodynamic and structural properties have been reviewed by Gabrielli et al., [3], Gaines [6], Langevin and Monroy [7], and the authors [1,4]. This review article focuses mainly on the experimental studies at equilibrium state, performed in the last two decades on the thermodynamic, structural, and dynamic dilational properties of binary polymer blend films spread at the water surface as a function of the miscibility of the polymer films. Non-equilibrium properties of polymer blend films should be important to fully understand about their physical behavior. When di- or triblock copolymers were spread at the air-water, their microsegregation provided interesting information [1,5,7] and then it should be useful to compare their interfacial behavior with the genuine blends formed by the same blocks. However, such comparisons have never been reported.

## 2. Measurement techniques

The interfacial characteristics of binary polymer blend films spread at the air-water interface are often discussed in terms of the miscibility of the polymer films in quasi-two dimensional spaces using surface pressure measurement techniques, fluorescence microscopy, ellipsometry, AFM, and dynamic dilational moduli measurement techniques [1,4,5,7].

### 2.1. Surface pressure measurements

A Langmuir trough attached to a Wilhelmy plate has been widely employed to measure surface pressure-surface area ($\pi$-$A$) isotherms of binary polymer blend films at the air-water interface. The polymer blend in a solution of volatile solvents is spread on the water surface in the trough and the solvent allowed evaporating. Measurements are usually undertaken at a fixed temperature by continuous or stepwise compression of the water surface, i.e. the compression method. In contrast, without compression of the water surface in the trough, the polymer blends are applied sequentially to the water surface with a fixed surface area in order to change the surface concentration $\Gamma$; this is called as the addition method. The difference between the compression method and the addition method for studying the $\pi$-$A$ isotherms is often observed at higher $\Gamma$ where the $\pi$ value measured by the former method should be gradually relaxed with time at fixed $A$.

For polymer films spread at the air-water interface, the term $A$ is generally expressed as the reciprocal of $\Gamma$ for the spreading polymer, i.e., with unit of $m^2$/mg. The $\Gamma$ value should correspond to the amount of adsorbed polymer at the air-water interface when neither desorption of the polymer from the interface nor dissolution of polymer into the water sub-phase occurs.

The properties of the binary polymer blend films depend on the properties of the individual polymer films spread at the air-water interface. Plots of $\pi$ as a function of the total surface concentration $\Gamma_{total}$ for a polymer blend film show dilute, semi-dilute, and concentrated regimes [1,4,5,7]. The surface overlapping concentration $\Gamma^*$ can be estimated by extrapolating a straight line from the plot of $\pi$ vs. $\Gamma_{total}$ to $\pi = 0$. The dilute and semi-dilute regimes are defined as the regions of the $\pi$ vs. $\Gamma_{total}$ plot below and above $\Gamma^*$, respectively. As $\Gamma_{total}$ increases, a semi-dilute regime in which double logarithmic plots of $\pi$ vs. $\Gamma_{total}$ are fitted with a power law defined by $\pi \propto \Gamma_{total}^{y}$ appears, where $y = 2\nu/(2\nu - 1)$ and $\nu$ is the critical exponent of the excluded volume of quasi-two dimensional spaces [8,9]. It is well known that the excluded volume effect depends strongly on the solvent conditions for polymer chains. The numerical values of $\nu$ under good and theta solvent conditions were calculated to be 0.77 ($y = 2.85$) [10] and 0.505 ($y = 101$) [11], respectively. When $\Gamma_{total}$ further increases beyond the semi-dilute regime, the $\pi$ value plateaus at a surface concentration of $\Gamma^{**}$ which marks the transition from the semi-dilute to the concentrated regime.

Moreover, the $\pi$ values of binary film containing polymers 1 and 2 are often plotted as a function of surface concentration, $\Gamma_1$ and $\Gamma_2$ for component 1 and 2, respectively, of the corresponding polymer blends to elucidate the influence of the surface concentration on the $\pi$ values.

### 2.2. Measurement of structural properties

Fluorescence microscopy and ellipsometry have been applied to binary polymer blend films spread at the air-water interface for investigation of their in situ interfacial structures. Moreover, techniques such as spectroscopy or surface potential are also useful to detect changes in the in situ interfacial structures of films on water surface. However, application of the corresponding methods to binary polymer blend films was hardly reported. In contrast, AFM allows indirect interpretation of the interfacial behavior and conformation of blended polymers in the films.

#### 2.2.1. Fluorescence microscopy

Fluorescence microscopy is used to analyze the interfacial morphology of polymer blend films spread at the air-water interface. A fluorescence probe material is added at a concentration of < 1 mol%, which is selectively soluble in the fluid (expanded) phase and insoluble in the condensed phase, in order to distinguish these phases by contrast differences in the microscopic images. However, all the polymers do not present expanded and condensed phases. Fluorescence microscopy measures the light reflected from an interface after irradiation with an excited laser beam or mercury light using a CCD (charge coupled device) or a SIT (silicon intensifier target) camera. However, as even the small amount of added fluorescence probe material can be regarded as an impurity in the spreading films, there are concerns as to whether the observed fluorescence images reflect real morphologies. In order to avoid the drawbacks of the fluorescence microscopy, Brewster angle microscopy (BAM) developed by two research groups in 1991 [12,13] is based on ellipsometry and is only governed by the refraction index.

#### 2.2.2. Ellipsometry

Ellipsometry is often used for analyzing adsorption kinetics and layers formed at various interfaces since it simultaneously provides the refractive index and the average thickness of the adsorbed and formed layers, assuming that the corresponding layers are homogeneous [14]. For an inhomogeneous polymer layer at the air-water interface, Rottke et al. have proposed that nulling-based ellipsometric mapping can be used to characterize its morphological inhomogeneity [15]. Ellipsometry is based on the measurement of changes in the ellipticity of polarized light caused by reflection at an interface. The ellipticity can be defined by the reflective phase difference $\Delta$ and the amplitude ratio tan $\Psi$ between two plane-polarized light waves, oscillating in parallel and perpendicular directions with respect to the incidence plane, as a function of the refractive index and the thickness of a layer. When the layer is thin, changes in $\Delta$ by the formation of layers at the interface are much easier to detect than changes in $\Psi$.

#### 2.2.3. AFM

AFM is the most commonly used scanning probe microscopy technique used to characterize nanoscale surface structures since it can be applied dielectrics, insulators, and soft materials. The AFM technique measures the deflection of a cantilever due to repulsive forces generated by interactions between sharp tip and the sample surface [16]. When the tip microscopically moves over the surface (in either contact or tapping mode), a force is generated causing deflection of the cantilever. This force is measured to provide an image of the surface. Thus, tapping

mode AFM has often been employed to characterize the surface topography of LB films of polymer blends. Moreover, AFM provides information on the mechanical properties of the film from the curves for friction or force against distance by contact mode.

### 2.3. Dynamic dilational measurements

In the oscillating barrier method, the barriers in a Langmuir trough are subjected to sinusoidal motion at constant angular frequency, where the strain curve should also follow a sinusoidal function. When such a strain is imposed on a film spread at an air-water interface after relaxation was applied to attain equilibrium π, the π value shows a linear response with a phase factor δ caused by viscous delay. The complex surface dilational modulus $E^*$ consists of a real part, the dynamic elasticity $E'$, and an imaginary part, the dilational viscosity $E''$ as shown in Eq. (2).

$$E^* = E' + iE'' \text{ and } |E^*| = \sqrt{E'^2 + E''^2} \quad (2)$$

Moreover, the shape of the Lissajous orbit of the plot of π vs. imposed strain shows whether the relationship between stress and stress is linear or non-linear.

In addition, other techniques are used, such as capillary wave methods that detect surface light scattering and excited wave techniques that probe the light scattered by thermally and externally excited transverse capillary waves, respectively. These techniques are based on the solution of the propagation of transverse capillary waves using the linearized Navier-Stokes equations under appropriate boundary conditions. Thus, at a given frequency, a relationship between $E^*$ and π, and the damping coefficient of the transverse capillary waves, has been derived using the hydrodynamic theory.

## 3. Miscible binary polymer blend films

Four binary polymer blend films have been shown to be miscible, according to the criterion given in Eq. (1); poly(ethylene oxide)–poly(methyl methacrylate) (PEO–PMMA) [17], poly(ethylene glycol)–poly(lactide-*co*-glycolide) (PEG–PLGA) [18], poly(vinyl acetate)–poly(4-hydroxystyrene) (PVAc–PHS) [19–21], and PVAc–poly(n-hexyl isocyanate) (PVAc–PHIC) [22–24]. PEO–PMMA and PEG–PLGA consist of water-soluble and water-insoluble polymers, whereas PVAc–PHS and PVAc–PHIC are formed by two water-insoluble polymers.

### 3.1. PEO–PMMA

Polymer blends of PEO and PMMA are known to be compatible in the bulk state due to their intermolecular hydrogen bonding [25]. Kato and Kawaguchi measured the dynamic dilational moduli of PEO–PMMA blend films using the oscillating barrier method, together with the respective polymer films [17]. The analysis of the π-*A* isotherms showed that the PEO is an expanded film, while the PMMA is a condensed film. Moreover, water is a good solvent and a solvent for PEO, whereas it is a near theta (poor) solvent for PMMA [1,4]. The PEO–PMMA blends, and pure PEO and PMMA films were all fully relaxed after spreading. At this point the dynamic dilational moduli were measured, as the π values of the PEO–PMMA blend and PMMA film measured by the continuous compression method at high surface concentrations of PMMA were larger than those measured by the relaxation method [17]. On the other hand, the structure of PEO containing ether bonds in the main chains should be fairly flexible and the π values of the PEO film were independent of the measurement technique [17].

Fig. 1 shows the equilibrium π values determined by the relaxation method for typical PEO–PMMA blends, pure PEO and PMMA films as a function of $\Gamma_{total}$ [17]. The π values at a fixed $\Gamma_{total}$ increase with decreasing molar fraction of PMMA $X_{PMMA}$ in the corresponding polymer blend films. In the plots, two plateau regions or inflection points are

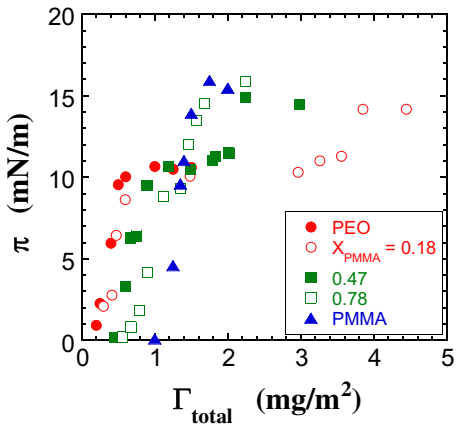


**Fig. 1.** Plots of surface pressure (π) determined by the surface pressure relaxation method as a function of total surface concentration ($\Gamma_{total}$) for PEO–PMMA blend films with $X_{PMMA}$ = 0.18 (red open circle), 0.47 (green filled square), and 0.78 (green open square), and pure PEO (red filled circle) and PMMA (blue filled triangle) films. (For interpretation of the references to colour in this figure legend, the reader is referred to the web version of this article.)

observed at the π values ca. 10 and 15 mN/m for the PEO and PMMA blend films, respectively. Moreover, the exponent *y* of the double logarithmic plots of π vs. $\Gamma_{total}$ (not shown here) increased with increasing with $X_{PMMA}$. These results indicate that PEO and PMMA are adsorbed at the air-water interface due to their miscibility even in the concentrated regimes.

In order to confirm whether the relationship between the imposed strain and the stress measured using the oscillating barrier method is linear or non-linear, the Lissajous orbit obtained by plotting π against the compression and expansion cycles is often used. The Lissajous orbits of the PEO–PMMA blend films strongly depend on the $\Gamma_{total}$, and an increase in this value is observed in the positive hysteresis loops of the Lissajous orbits as a change from a crossover loop to a negative loop, irrespective of the composition; below a surface concentration of $\Gamma_{PMMA}$ = 1.0 mg/m$^2$ every Lissajous orbit exhibited a positive loop, whereas above $\Gamma_{PMMA}$ = 1.3 mg/m$^2$ every Lissajous orbit exhibited a negative loop. PEO films showed positive hysteresis loops in the Lissajous orbits, irrespective of the surface concentration. PMMA at a surface concentration of 1.35 mg/m$^2$ showed a cross over hysteresis loop. A negative hysteresis loop occurred during compression cycles below $A/A_0$ = 1.03, and a positive hysteresis loop occurred above this value during an expansion loop, where *A* and $A_0$ are the surface area at a given strain and zero strain, respectively [17].

Fig. 2 shows the Lissajous orbits of the PEO–PMMA blend with $X_{PMMA}$ = 0.47, pure PEO and PMMA films, for π ≈ 10 mN/m at zero strain, an imposed sinusoidal oscillatory strain amplitude $u_0$ = 10%, and a fixed frequency of 20 mHz over 200 s [17]. The Lissajous orbits of PEO film are almost linear responses and those of PMMA and PEO–PMMA blend films correspond to non-linear responses though they are almost superimposed for repeating cycles. Such non-linear responses were intensively focused by Hiles et al. [26], Langevin and Monroy [7], Higuera et al. [27], and Bykov et al. [28], but we will not discuss it further in this review. Thus, the apparent dilational modulus $E_{app}$ for the PMMA and PEO–PMMA blend films is determined from the first cycle of the Lissajous orbits using Eq. (3).

$$E_{app} = \Delta\pi/u_0 \quad (3)$$

where Δπ is the difference between the maximum and the minimum π values for a given $u_0$.

Fig. 3 shows typical plots of $E_{app}$ for standard PEO–PMMA blends and pure PMMA films and $E^*$ for pure PEO film, as a function of $\Gamma_{total}$ [17]. It can be seen that the $E_{app}$ values of all blend films are lower than those of the PMMA film and higher than $E^*$ of the PEO film at a fixed $\Gamma_{total}$. An increase in $\Gamma_{total}$ leads to an increase in $E_{app}$ until it reaches a

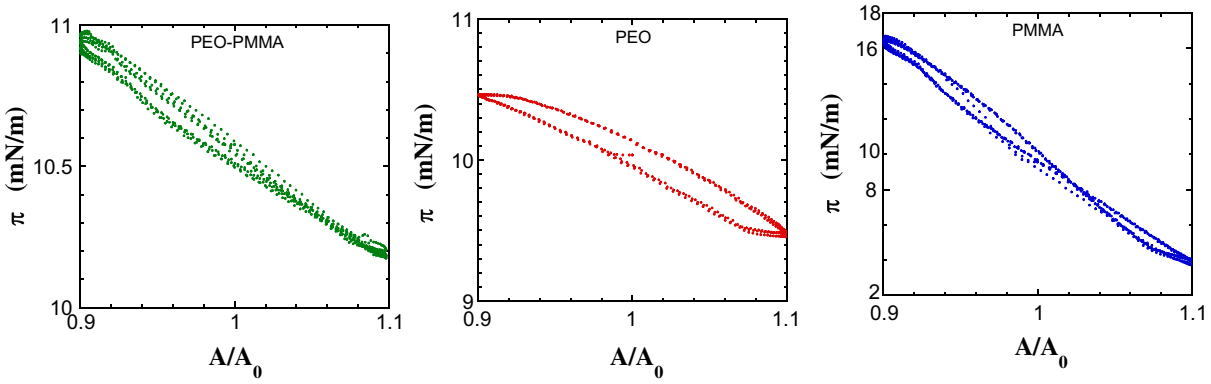


**Fig. 2.** Typical Lissajous orbits of PEO–PMMA blend film with $X_{PMMA}$ = 0.47 (green), and pure PEO (red) and PMMA (blue) films at the strain of 10% and the fixed frequency of 20 mHz during 200 s. (For interpretation of the references to colour in this figure legend, the reader is referred to the web version of this article.)

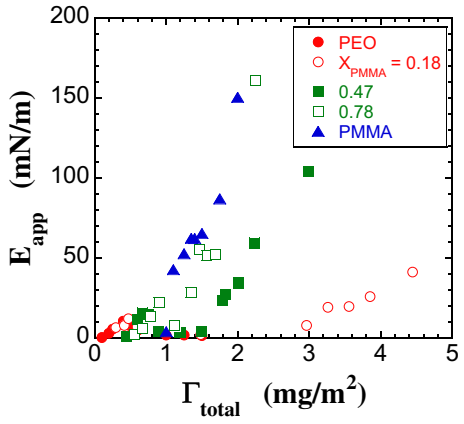


**Fig. 3.** Plots of $E_{app}$ of PEO–PMMA blend films with $X_{PMMA}$ = 0.18, 0.47, and 0.78, and pure PMMA films and $E^*$ of pure PEO. Symbols are the same as in Fig.1.

maximum value, after which it decreases. Further increasing $\Gamma_{total}$ above 1.0 mg/m$^2$ results in a steep increase in $E_{app}$, irrespective of $X_{PMMA}$ due to the expanded character of the film spread at the air-water interface. Moreover, the maximum $E_{app}$ of the blend film is located at a higher $\Gamma_{total}$ with increasing $X_{PMMA}$. Both the dependence of $E_{app}$ on $\Gamma_{total}$ above $\Gamma_{total}$ = 1.0 mg/m$^2$ and of $E_{app}$ on $X_{PMMA}$ also indicate that the PEO and PMMA chains are miscible at the air-water interface.

### 3.2. PEG–PLGA

PLGA has been widely investigated for sustained delivery systems for proteins [29,30] and the behavior and conformation of binary polymer blend films of PEG and PLGA were determined by measurements of π, dilational moduli, and the microstructures (by AFM) [18]. The corresponding binary polymer blend films were miscible at least in the range of π = 0–7 mN/m [18], where water is a good solvent for the respective polymer films.

The dilational moduli of the PEG–PLGA blend films spread at the air-water interface were measured using the π relaxation technique and $\Delta\pi_s$ was expressed by the sum of an equilibrium part $\Delta\pi_e$ and a non-equilibrium part $\Delta\pi_{ne}$. Moreover, the $\Delta\pi_e$ and $\Delta\pi_{ne}$ terms can be related to the equilibrium dilational elasticity $E_e$ and viscoelastic part of the dilational elasticity $E_{ne}$ as functions of the relaxation time $\tau$ based on a parallel combination of the elastic spring model and the Maxwell model, respectively, as shown in Eq. (4) [18].

$$\Delta\pi_s = \Delta\pi_e + \Delta\pi_{ne} = E_e\left(\frac{\Delta A}{A_i}\right) + E_{ne}\frac{\tau}{t}(1 - e^{-t/\tau})\left(\frac{\Delta A}{A_i}\right) \quad (4)$$

where $A_i$ is the initial surface area and $\Delta A/A_i$ is the corresponding strain. At π = 6 mN/m for the PEG–PLGA blend film with $X_{PLGA}$ = 0.39 the $E_e$ and $E_{ne}$ values were determined to be 4.7 and 8.8 mN/m, respectively. The sum of the $E_e$ and $E_{ne}$ values was close to that of the PEG film and less than that of PLGA film at the same π, while the PLGA film exhibited pure elastic behavior with no viscoelastic response. This may reflect the tendency of the PEG polymer chains to remain in their original state in the mixed film.

The static surface dilational elasticity $\varepsilon$ of PEG–PLGA blend films was also calculated using the following simple equation as a function of π for various $X_{PLGA}$:

$$\varepsilon = -A(\partial\pi/\partial A)_T = \Gamma\,(\partial\pi/\partial\Gamma)_T \quad (5)$$

The resulting $\varepsilon$ values for the polymer blend films were dependent on the PEG concentration in the mixed films. The maximum $\varepsilon$ value observed at π = 5 mN/m was almost independent of $X_{PLGA}$, and the minimum $\varepsilon$ value observed at π = 7 mN/m indicating the collapse of the PEG film was not dependent on $X_{PLGA}$. In addition, another $\varepsilon$ peak was observed at π = 10 mN/m, which was neither related to the PEG behavior nor to the PLGA behavior. Moreover, AFM images of the PEG–PLGA blend films deposited on mica surfaces allowed an understanding of their miscibility, namely the organization of the miscible polymer blend.

### 3.3. PVAc–PHS

Water is a good solvent for PVAc films, whereas it is a poor solvent for PHS films [19]. In contrast, the hydrogen bonds between the carbonyl groups in PVAc and the hydroxyl groups in PHS provide their miscibility. Monroy et al. measured π as a function of $\Gamma_{total}$ and calculated $\varepsilon$ values for PVAc–PHS blend films spread at the air-water interface at a pH of 2 as a function of the weight fraction of PVAc $x_{PVAc}$ in the corresponding polymer blend films [19]. The water sub-phase at a pH of 2 prevented hydrolysis of the hydroxyl groups of PHS. The $\nu$ value evaluated from the double logarithmic plots of π against $\Gamma_{total}$ increased with increasing $x_{PVAc}$ and a change from near theta solvent to good solvent was observed.

The resulting $\varepsilon$ values of the PVAc–PHS blend films showed a first maximum at a low $\Gamma_{total}$ value, which was strongly related to the rigidity of PVAc as a function of $x_{PVAc}$, until $x_{PVAc}$ was > 0.5. Above an $x_{PVAc}$ of 0.3, the second maximum in the $\varepsilon$ values was observed at a high $\Gamma_{total}$.

Monroy et al. subsequently measured π–$\Gamma_{total}$ isotherms and dilational moduli of PVAc–PHS blend films spread on a water sub-phase with a pH of 2 as a function of the molar fraction of PVAc $X_{PVAc}$ [20]. The $\varepsilon$ values in the dilute, semi-dilute, and concentrated regimes were calculated from Eq. (5) and the dilational moduli in the corresponding regimes were analyzed using capillary wave methods detecting surface light scattering.

The resulting $E'$ for the PVAc–PHS blend films in the dilute and semi-dilute regimes was slightly larger than the $\varepsilon$ values and showed a

maximum in the semi-dilute regime due to their expanded nature, irrespective of the $X_{PVAc}$. Moreover, the $\Gamma_{total}$ at which the maximum $E'$ value was observed increased with decreasing $X_{PVAc}$ and the curve was similar to that for the PEO–PMMA blend films [17]. The $E'$ value in the concentrated regime decreased with increasing $\Gamma_{total}$ and increased with increasing $X_{PVAc}$ and was lower than the $\varepsilon$ value, irrespective of $X_{PVAc}$. On the other hand, the $E''$ value increased with both $\Gamma_{total}$ and $X_{PVAc}$ and the increase in $E''$ with $\Gamma_{total}$ was almost independent of $X_{PVAc}$.

Rivillon et al. performed $\pi$–$\Gamma_{total}$ isotherm, ellipsometry, and dilational moduli measurements of PVAc–PHS blend films spread at the air-water interface at a pH of 2 as a function of $X_{PVAc}$ [21]. Their dilational moduli were measured using the relaxation method, oscillating barrier method, capillary wave methods detecting surface light scattering and excited wave techniques, which allowed analysis over a broad frequency range. In addition to the estimation of $\nu$ from the$\pi$–$\Gamma_{total}$ isotherms, analysis of $\Gamma^{**}$ gave the surface pressure $\pi^{**}$ at $\Gamma^{**}$ which decreased with increasing $X_{PVAc}$ up to a value $\approx 0.3$.

Ellipsometric changes in $\delta\Delta = (\Delta_0 - \Delta)$ by spreading of the polymer films at the air-water interface were much more sensitive than those in $\delta\Psi = (\Psi_0 - \Psi)$, as mentioned previously, where $\Delta_0$ and $\Psi_0$ are for pure water and $\Delta$ and $\Psi$ are for the water surface covered by the polymers [1]. The resulting $\delta\Delta$ linearly increased with increasing $\Gamma_{total}$, irrespective of $X_{PVAc}$, indicating that all spread polymer films are sat on water surface without desorption, whereas the amplitude of $\delta\Psi$ was much smaller than that of $\delta\Delta$ and was clearly not dependent on $\Gamma_{total}$. Moreover, the dependence of the ellipsometric thickness on $\Gamma_{total}$ was similar to $\delta\Delta$ and the thickness at $\Gamma^{**}$ increased with increasing $X_{PVAc}$, showed a maximum at $X_{PVAc} \approx 0.3$, and then decreased. On the other hand, the resulting $\delta\Delta$ for PEO films spread at the air-water interface linearly increased with increasing the spread amount of PEO up to its plateau $\pi$ and levelled off beyond the plateau $\pi$ since PEO is soluble in water [31].

Rivillon et al. only measured the dilational moduli of the PVAc–PHS blend films at $\Gamma^{**}$. In the low-frequency region, examined by the relaxation method and the oscillating barrier method, the measured dilational moduli showed a wide relaxation process [21]. The relaxation behavior of the PVAc-rich blend films has been described by the reptation of polymer chains at the interface and the diffusive adsorption-desorption dynamics of loops and tails [32], while no detailed explanation of the relaxation processes of PSH-rich blend films has yet been published.

In the high-frequency region studied by capillary wave methods, the PVAc-rich blend films showed two relaxation processes, at around 500 Hz and 40 kHz, whereas the PSH-rich blend films exhibited only a broad relaxation mode below 1 kHz.

### 3.4. PVAc–PHIC

PHIC is a helical, semi-flexible polymer [33] and water is a poor solvent for PHIC [34]. Kawaguchi's group investigated the interfacial characteristics of PVAc–PHIC blend films spread at air–water interfaces as a function of $X_{PVAc}$, using the compression method and fluorescence microscopy [22], AFM [23], and the oscillating barrier method [24].

Since fluorescence microscopy images of PVAc films in the presence of the fluorescence probe N-(7-nitro-2, 1,3-benzoxadiazol-4-yl)-L-a-dipalmitoyl phosphatidyl ethanol amine (NBD−PE) were almost isotropic, this technique was suitable for exploring the miscibility of PVAc–PHIC blend films [22]. Fig. 4 shows typical fluorescence microscopy images of pure PVAc at $\Gamma = 0.57$ mg/m$^2$, pure PHIC at $\Gamma = 0.76$ mg/m$^2$, and PVAc–PHIC blend films with $X_{PVAc} = 0.2$, 0.33, and 0.5 at a fixed $\Gamma_{PHIC}$ of 0.76 mg/m$^2$ [22]. With the exception of the PHIC film, the surface concentrations in PVAc and PVAc–PHIC blend films were in the semi-dilute regimes of the respective polymer films. The dark areas in the fluorescence microscopy images of the polymer blend films increased with increasing $X_{PVAc}$. This also guarantees that PVAc and PHIC are miscible at the air-water interface. If the corresponding polymer blends are immiscible, PVAc should be preferentially adsorbed on the water surface due to chain flexibility and stable film formation and part of the PHIC should be repelled, leading to a uniform image.

Fig. 5 shows AFM images [23] of LB films of PHIC–PVAc blend films with $X_{PVAc} = 0.2$, 0.5, and 0.67 at a fixed surface area of 0.5 nm$^2$/average repeating unit, at $\Gamma_{total} = 0.39$, 0.35, and 0.33 mg/m$^2$, respectively, which are dilute regimes in the blend films. An AFM image of a pure PHIC film at $\Gamma = 0.42$ mg/m$^2$ is also shown. An increase in $X_{PVAc}$ in the blend film induces changes in the grain structures from connected partially lost coils to extended bundled rods. The resulting AFM image was thought to show mainly the PHIC component, since no AFM image of the LB film of PVAc was observed at the corresponding surface concentration of PVAc in the polymer blend films. Thus, it makes sense that the bright areas in the AFM images decrease with increasing $X_{PVAc}$. The calculated fraction of the bright areas in the AFM image decreases to 0.74, 0.45, and 0.37 with increasing $X_{PVAc}$, and the respective figures almost correspond with $X_{PHIC} = 1 - X_{PVAc}$ in the polymer blend films.

Morioka and Kawaguchi measured $\pi$–$\Gamma_{total}$ isotherms for PHIC–PVAc blend films with $X_{PVAc} = 0.1$, 0.33, 0.5, and 0.8 as a function of $\Gamma_{total}$ [24]. The $y$ value of the double logarithmic plot of $\pi$ against $\Gamma_{total}$ (not shown here) decreased with increasing $X_{PVAc}$. Moreover, they measured $E_{app}$ values for PHIC–PVAc blend films as a function of $\Gamma_{total}$ since Lissajous orbits for most of the corresponding blend films showed a non-linear response [24]. The resulting $E_{app}$ values are shown in Fig. 6 [24], plotted on a double logarithmic graph as a function of $\Gamma_{total}$ at a fixed strain of 10%. Below $\Gamma_{total} = 1.0$ mg/m$^2$, where all blend films are in the semi-dilute regime, the $E_{app}$ values increase with increasing $\Gamma_{total}$, irrespective of $X_{PVAc}$, and their magnitude at a fixed $\Gamma_{total}$ increases with increasing $X_{PVAc}$. Above $\Gamma_{total} = 1.0$ mg/m$^2$ the $E_{app}$ values also increase with increasing $\Gamma_{total}$ and their magnitudes show no $X_{PVAc}$ dependence. Moreover, the plots of $E_{app}$ vs. $\Gamma_{total}$ in the semi-dilute regime approximately followed a power law of $E_{app} \propto \Gamma_{total}^{n}$ [20] with the exponent $n$ decreasing with increasing $X_{PVAc}$, indicating that the PVAc–PHIC blend films gradually changed from a glass-like material to expanded films.

It can be concluded that there are some common features, namely the exponent $y$ for $\pi$–$\Gamma_{total}$ isotherms, the plateau $\pi$, and the surface dilational moduli that depend on the blend ratio, irrespective of the miscible polymer blends.

## 4. Immiscible binary polymer blend films

Two binary polymer blend films, PVAc–PEO [35] and PVAc–PMMA [36], have been shown to be immiscible according to the criterion given by Eq. (1). PVAc–poly(methyl acrylate) (PMA) binary blends have been regarded as an ideal binary mixture because their mean surface areas lay almost on the additive line defined by Eq. (1) and their chemical structures are similar [37]. However, both $\pi$ measurements at high $\Gamma_{total}$ ranges and ellipsometric results of the PVAc–PMA blend films showed that they were immiscible in a two-dimensional phase due to the preferential adsorption of PVAc on the water surface [38]. Moreover, PVAc–poly(dimethylsiloxane) (PDMS) binary blends have been classified as a miscible polymer blend film according to Eq. (1) [39]. However, evidence for strong miscibility of the corresponding blend films could be excluded from a proposed simple rule adding $\pi$, $E'$, and $E''$, and it was concluded that PVAc and PDMS formed a bilayer structure on the water surface where a PDMS layer was laid on top of a PVAc layer. PVAc–PEO consists of water-soluble and water-insoluble polymers, whereas PVAc–PMMA, PVAc–PMA, and PVAc–PDMS are formed by two water-insoluble polymers.

### 4.1. PVAc–PEO

Yoshida and Kawaguchi measured $\pi$ and the dynamic dilational

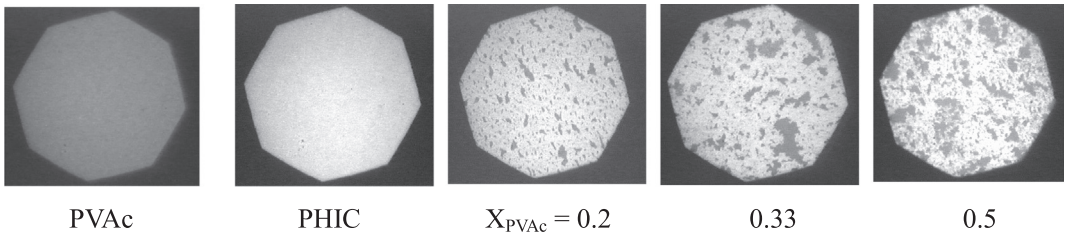


**Fig. 4.** Typical fluorescence microscopy images of pure PVAc, pure PHIC, and PVAc–PHIC blend films with $X_{PVAc}$ = 0.2, 0.33, and 0.5.

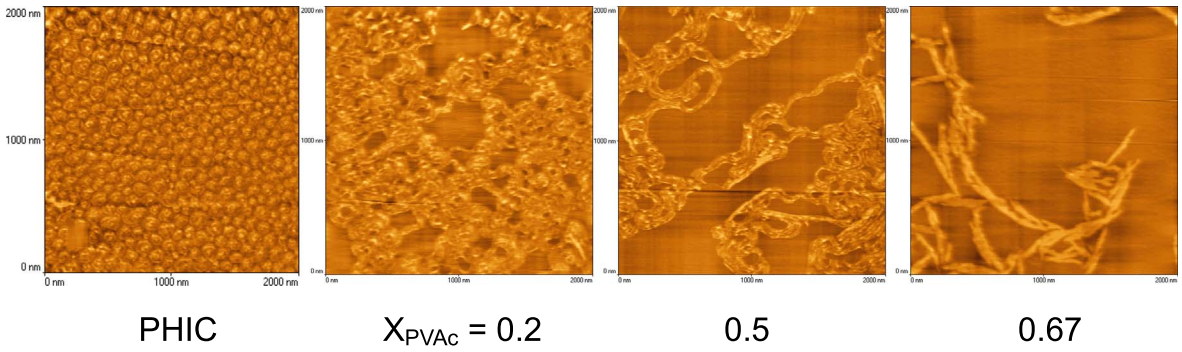


**Fig. 5.** Typical AFM images of pure PHIC and PVAc–PHIC blend films with $X_{PVAc}$ = 0.2, 0.5, and 0.67. The size of the respective images is 2 × 2 μm$^2$.

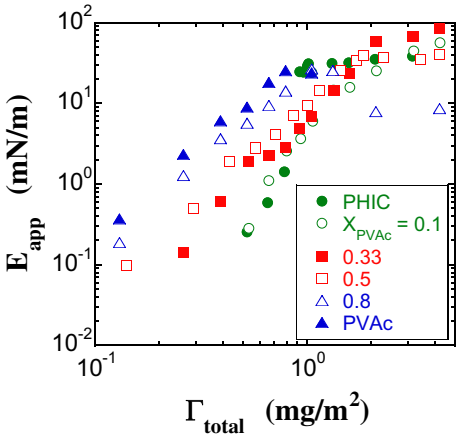


**Fig. 6.** Double logarithmic plots of $E_{app}$ of PVAc–PHIC blend films with $X_{PVAc}$ = 0.1 (green open circle), 0.33 (red filled square), 0.5 (red open square), and 0.8 (blue open triangle), and pure PHIC (green filled circle) and PVAc (blue filled triangle) films. (For interpretation of the references to colour in this figure legend, the reader is referred to the web version of this article.)

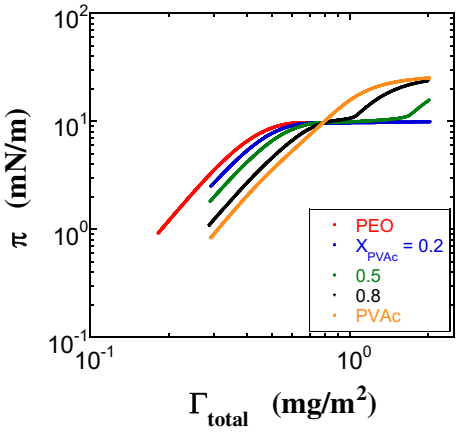


**Fig. 7.** Double logarithmic plots of surface pressure (π) as a function of total surface concentration ($\Gamma_{total}$) for PVAc–PEO blend films with $X_{PVAc}$ = 0.2 (blue), 0.5 (green), and 0.8 (black), and pure PEO (red) and PVAc (orange) films. (For interpretation of the references to colour in this figure legend, the reader is referred to the web version of this article.)

moduli of PVAc–PEO blend films using the oscillating barrier method, along with pure PVAc and PEO films [35]. The π values of all films were measured using the continuous compression method since relaxation of π was not observed due to both polymer films being expanded types.

Fig. 7 shows double logarithmic plots of π values for typical PVAc–PEO blends, and pure PVAc and PEO films, as a function of $\Gamma_{total}$ [35]. The plots in the semi-dilute regimes are fitted with a power law defined by $\pi \propto \Gamma_{total}^{\ y}$, where $y$ = 2.64, irrespective of the film type. The π values of the PVAc–PEO blend films at a fixed $\Gamma_{total}$ in the semi-dilute regime increase with increasing $X_{PVAc}$; beyond the semi-dilute regime they show the opposite behavior. In the plots for the PVAc–PEO blend films, an inflection point is observed at π values ca. 10 mN/m, which corresponds to the plateau π value of PEO. These results indicate that PEO is preferentially adsorbed over PVAc at the air-water interface due to the immiscibility of the two polymers.

Fig. 8 shows Lissajous orbits of the PVAc–PEO blend with $X_{PVAc}$ = 0.5, and pure PVAc and PEO films for π = 8 mN/m at zero strain, $u_0$ = 10%, and a fixed frequency of 20 mHz over 200 s [35]. All Lissajous orbits exhibit positive hysteresis loops which are almost superimposed for repeating circles and they correspond to linear responses. Moreover, the Lissajous orbits have similar shapes, irrespective of the film type, and are independent of π at values < 8 mN/m, where the respective films are in the semi-dilute regime. Thus, the $E^*$ values of the PVAc–PEO blends, and pure PVAc and PEO films are determined from the first cycle of the Lissajous orbits using Eq. (3).

Fig. 9 shows plots of $E^*$ for typical PVAc–PEO blends, and pure PVAc and PEO films, as a function of $\Gamma_{total}$ [35]. An increase in $\Gamma_{total}$ leads to an increase in $E^*$ until it reaches a peak value, after which it decreases (except for the pure PVAc film). This peak increases with increasing $X_{PVAc}$. The presence of the peak can be mainly attributed to the PEO in the films, indicating that PEO chains are preferentially adsorbed on the water surface.

### 4.2. PVAc–PMMA

Mitsui et al. measured the dynamic dilational moduli of

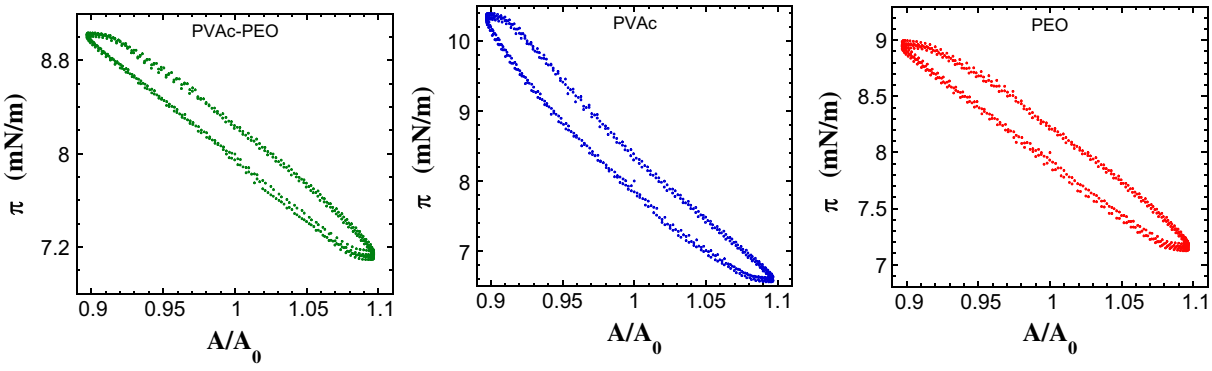


**Fig. 8.** Typical Lissajous orbits of PVAc–PEO blend film with $X_{PVAc}$ = 0.5 (green), and pure PVAc (orange) and PEO (red) films at the strain of 10% and the fixed frequency of 20 mHz during 200 s. (For interpretation of the references to colour in this figure legend, the reader is referred to the web version of this article.)

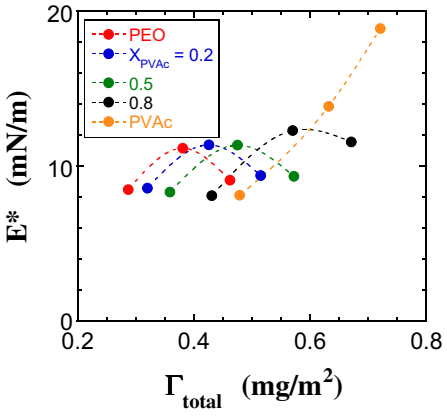


**Fig. 9.** Plots of $E^*$ of PVAc–PEO blend films with $X_{PVAc}$ = 0.2 (blue), 0.5 (green), and 0.8 (black), and pure PEO (red) and PVAc (orange) films. (For interpretation of the references to colour in this figure legend, the reader is referred to the web version of this article.)

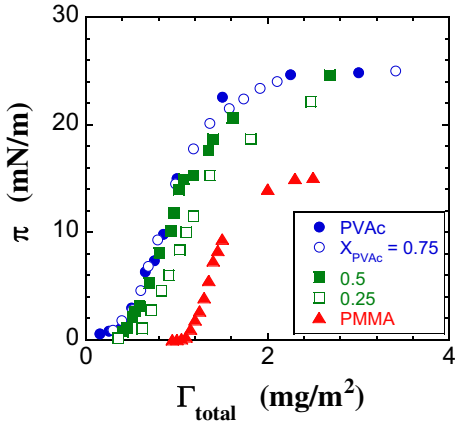


**Fig. 10.** Plots of surface pressure (π) as a function of total surface concentration ($\Gamma_{total}$) for PVAc–PMMA blend films with $X_{PVAc}$ = 0.25 (green open square), 0.5 (green filled square), and 0.75 (blue open circle), and pure PVAc (blue filled circle) and PMMA (red filled triangle) films. (For interpretation of the references to colour in this figure legend, the reader is referred to the web version of this article.)

PVAc–PMMA blend films, and pure PVAc and PMMA films using the oscillating barrier method [36]. All the PVAc–PMMA blend and PMMA films were fully relaxed after spreading since the π values measured by the continuous compression method (at $\Gamma_{PMMA}$ values above 1.5 mg/m$^2$) were larger than those measured by the relaxation method. Thus, the dynamic dilational moduli of the PVAc–PMMA blends, and the PVAc and PMMA films, were measured after their equilibrium π values were attained. The resulting Lissajous orbits were almost superimposed for repeating cycles and they showed linear responses.

Fig. 10 shows the equilibrium π values for typical PVAc–PMMA blends, and pure PVAc and PMMA films as a function of $\Gamma_{total}$ [36]. The π values at a fixed $\Gamma_{total}$ increase with increasing $X_{PVAc}$ and the plateau π values for the PVAc–PMMA blend films are similar to that of the PVAc film since PVAc is preferentially adsorbed on the water surface. These results suggest that PVAc and PMMA are immiscible at the air-water interface. Above $\Gamma^*$, double logarithmic plots of π vs. $\Gamma_{total}$ (not displayed) are fitted to $\pi \propto \Gamma_{total}^{y}$ and it is observed that $y$ increases with decreasing $X_{PVAc}$. Although the exponent of $y$ for the miscible PVAc–PHS blends increased with decreasing $X_{PVAc}$, their plateau π values were dependent of $X_{PVAc}$ [21].

Fig. 11 shows plots of $E^*$ for all PVAc–PMMA blends, and the pure PVAc and PMMA films, as a function of $\Gamma_{total}$ [36]. The resulting $E^*$ values of the polymer blend films are lower than those of the PMMA film and higher than those of the PEO film at a fixed $\Gamma_{total}$. An increase in $\Gamma_{total}$ leads to an increase in $E^*$ until it reaches a peak value, after which it decreases, irrespective of $X_{PVAc}$. The $E^*$ values below and above the peak increase and decrease with increasing $X_{PVAc}$, respectively, irrespective of $X_{PVAc}$. Thus, the decrease in $E^*$ with further increase of $\Gamma_{total}$ above the position of the peak indicates that PVAc is preferentially adsorbed over PMMA at the air-water interface, i.e., these

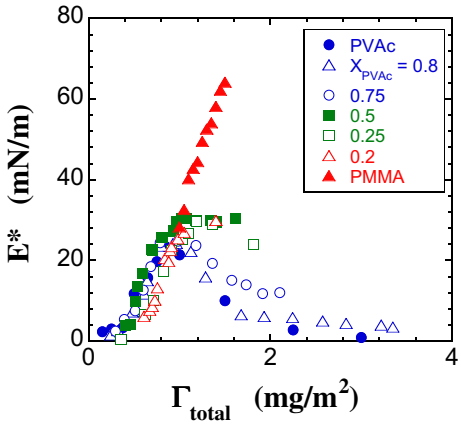


**Fig. 11.** Plots of $E^*$ of PVAc–PMMA blend films with $X_{PVAc}$ = 0.2 (red open triangle), 0.25, 0.5, 0.75, and 0.8 (blue open square), and pure PVAc and PMMA films. Symbols are the same as in Fig.10. (For interpretation of the references to colour in this figure legend, the reader is referred to the web version of this article.)

polymers are immiscible. Moreover, the peak in $E^*$ of the polymer blend film is located at higher $\Gamma_{total}$ values as $X_{PVAc}$ decreases.

### 4.3. PVAc–PMA

Kawaguchi et al. thoroughly investigated PVAc–PMA blend films spread at the air-water using π measurements and ellipsometry [38] and they subsequently carried out AFM analysis (tapping mode) of the

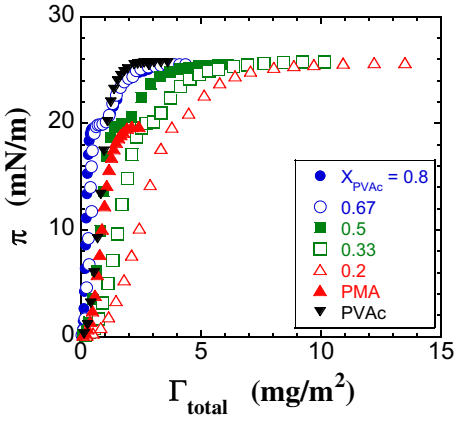


**Fig. 12.** Plots of surface pressure (π) as a function of total surface concentration ($\Gamma_{total}$) for PVAc–PMA blend films with $X_{PVAc}$ = 0.2 (red open triangle), 0.33 (green open square), 0.5 (green filled square), 0.67 (blue open circle), and 0.8 (blue filled circle), and pure PMA (red filled triangle) and PVAc (black filled anti-triangle) films. (For interpretation of the references to colour in this figure legend, the reader is referred to the web version of this article.)

LB polymer blend films deposited on mica surfaces [40].

Their measurements of π at $\Gamma_{total}$ values above 2.0 mg/m$^2$ resulted in the conclusion that PVAc–PMA blend films spread at the air-water were immiscible since their π–$\Gamma_{total}$ plots gave similar plateau surface pressures to that of the pure PVAc film, irrespective of $X_{PVAc}$, as shown in Fig. 12 [38]. Moreover, the ellipsometric studies of changes in δΔ for the PVAc–PMA blend films as a function of PVAc and PMA concentrations showed that the polymer blend films were immiscible. The resulting δΔ values for spreading PVAc at $\Gamma_{PVAc}$ = 1.0 mg/m$^2$ (where the film was in the semi-dilute regime) and subsequent spreading of PMA at various $\Gamma_{PMA}$ of 0.25, 1.0, and 4.0 mg/m$^2$ were similar to those for spreading pure PVAc at $\Gamma_{PVAc}$ = 1.0 mg/m$^2$. Changes in the order in which the polymers were spread on water resulted in the same δΔ values as measured at the fixed $\Gamma_{PVAc}$ of 1.0 mg/m$^2$. This was attributed to the preferential adsorption of PVAc on the water surface, where previously adsorbed PMA on the water surface was completely displaced by PVAc.

AFM images of the LB binary blend films of PVAc–PMA also provided evidence for the immiscibility of these polymer blend films [40]. Fig. 13 shows AFM images of PVAc–PMA blend films for $X_{PVAc}$ = 0.67, 0.5, and 0.33 at a fixed $\Gamma_{PVAc}$ = 1.0 mg/m$^2$ [40]. The granule population is higher and some granules grow to heights > 10 nm with increasing $\Gamma_{PMA}$. These changes in the topography support the hypothesis that the binary blend films of PVAc–PMA are immiscible.

### 4.4. PVAc–PDMS

Runge and Yu extensively investigated PVAc–PDMS blend films spread at the air-water as a function of $X_{PVAc}$, using π measurements and the capillary wave method detecting surface light scattering [39]. The π-$A$ isotherms for these blend films showed strong negative deviations from Eq. (1), indicating that the PVAc–PDMS blend films were miscible on the water surface. They proposed an additive surface pressure model (as given by Eq. (6)) based on the two-dimensional analog of Dalton's law of partial pressures for an ideal gas mixture, and compared the model with their experimental results.

$$\pi(\langle A\rangle) = \pi_1(A_1) + \pi_2(A_2),\ \langle A\rangle^{-1} = A_1^{-1} + A_2^{-1},\ A_i^{-1} = X_i/\langle A\rangle \tag{6}$$

where $\pi_1(A_1)$ and $\pi_2(A_2)$ are the surface pressures at the surface areas $A_1$and $A_2$ for polymers 1 and 2, respectively. The calculated $\pi(\langle A\rangle)$ values were in close agreement with the measured π values, except at the plateau region where the modeled values were larger than the experimental ones. The success of the model allowed interactions between polymer chains to be neglected and no excluded area effects in the dilute and semi-dilute regimes were observed, leading to the proposal that PDMS was partially spread on the PVAc film forming a bilayer structure at the limiting area in the polymer blend film. This indicates that PVAc–PDMS blend films spread at the air-water interface are in the immiscible state.

Moreover, Runge and Yu also extended the concept of surface pressure defined by Eq. (6) to the quantities of $E'$ and $E''$ and compared the calculated and measured values [39]. In this case, the experimental values were clearly different to the calculated ones; however, the dependence of the calculated $E'$ and $E''$ values on $\langle A\rangle$ showed similar trends to the measured curves.

It can be concluded that there are some common features, namely the exponent $y$ for π–$\Gamma_{total}$ isotherms that are independent of the polymer blend ratio and the surface dilational moduli are governed by the preferentially adsorbed polymer component, irrespective of the immiscible polymer blends.

## 5. Conclusions

This review describes the current status of experimental studies of binary polymer blend films spread at the air-water interface. Binary polymer blend films are characterized by measuring π–surface concentration isotherms, interfacial structures, and dynamic dilational moduli as a function of miscibility.

For miscible binary polymer blend films, the respective polymer components are adsorbed on the water surface even if their surface concentrations are in the semi-dilute and concentrated regimes. Hence, the π values, microstructures, and dilational moduli show strong dependence on the molar fraction of the respective components at the air-water interface.

On the other hand, the interfacial properties of immiscible binary polymer blend films in the semi-dilute and concentrated regimes are similar to those of one component, which is preferentially adsorbed over other component at the air-water interface. However, further studies of binary polymer blend films are needed to gain a deep understanding of the interfacial structures and dilational moduli of the films and the relationship between their interfacial properties and miscibility.

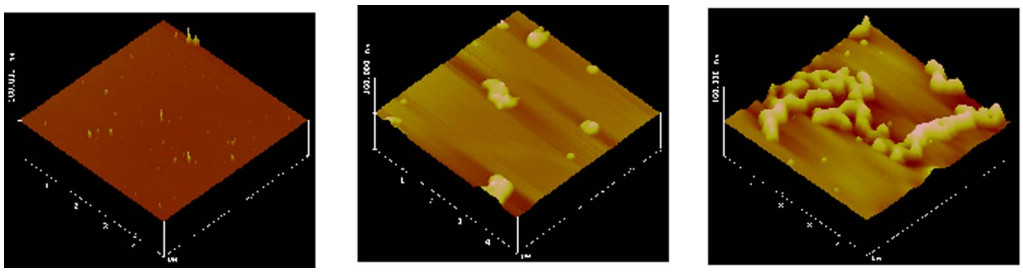


**Fig. 13.** Typical AFM images of PVAc–PMA blend films with $X_{PVAc}$ = 0.67, 0.5, and 0.33. The size of the respective images is 5 × 5 × 0.04 μm$^3$.

## References


[1] Kawaguchi M. Thermodynamic, structural and rheological properties of polymer films at the air-water interface. Prog Polym Sci 1993;18:341–76.
[2] Ries Jr. HE, Walker DC. Films of mixed horizontally and vertically oriented compounds. J Colloid Sci 1661;16:361–74.
[3] Gabrielli G, Puggelli M, Baglioni P. Orientation and compatibility in monolayers. J Colloid Interface Sci 1982;86:485–500.
[4] Kawaguchi M. Thermodynamic and structural properties of polymer thin films at interfaces. In: Ariga K, Nalwa S, editors. Bottom-up nanofabrication. Stevenson ranch: Am Sci Pub; 2009. p. 299–320.
[5] Morioka T, Kawaguchi M. Surface dilational moduli of polymer and blended polymer monolayers spread at air-water interfaces. Adv Colloid Interface Sci 2014;214:1–16.
[6] Gaines Jr. GL. Monolayers of polymers. Langmuir 1991;7:834–9.
[7] Langevin D, Monroy F. Interfacial rheology of polyelectrolytes and polymer monolayers at the air-water interface. Curr Opin Colloid Interface Sci 2010;15:283–93.
[8] Ober R, Vilanove R. Surface pressure of polyvinyl acetate monolayers at the air water interface: new data and comparison with the scaling theory. Colloid Polym Sci 1977;255:1067–73.
[9] Vilanove R, Rondelez F. Scaling description of two-dimensional chain conformations in polymer monolayers. Phys Rev Lett 1980;45:1502–5.
[10] Le Guillou JC, Zinn-Justin J. Critical exponents for the n-vector model in three dimensions from field theory. Phys Rev Lett 1977;39:95–8.
[11] Stephen MJ, McCauley Jr. JL. Feynman graph expansion for tricritical exponents. Phys Lett A 1973;44A:89–90.
[12] Hénon D, Meunier J. Microscope at the Brewster angle: direct observation of first-order phase transitions in monolayers. Rev Sci Instrum 1991;62:936–9.
[13] Hönig D, Möbius D. Direct visualization of monolayers at the air-water by Brewster angle microscopy. J Phys Chem 1991;95:4590–2.
[14] Rothen A. The ellipsometer, an apparatus to measure thickness of thin surface films. Rev Sci Instrum 1945;16:26–30.
[15] Rottke FO, Schulz B, Richau K, Kratz K, Lendlein A. An ellipsometric approach towards the description of inhomogeneous polymer-based Langmuir layers. Beilstein J Nanotechnol 2016;7:1156–65.
[16] Binnig G, Quate CF, Gerber Ch. Atomic force microscope. Phys Rev Lett 1986;56:930–3.
[17] Kato S, Kawaguchi M. Surface dilational moduli of poly(ethylene oxide), poly (methyl methacrylate), and their blend films. J Colloid Interface Sci 2012;384:87–93.
[18] Malzert A, Boury F, Saulnier P, Benoit JP, Proust JE. Interfacial properties of mixed polyethylene glycol/poly(D,L-lactide-co-glycolide) films spread at the air-water interface. Langmuir 2000;16:1861–7.
[19] Monroy F, Esquinas MJ, Ortega F, Rubio RG. Monolayers of hydrogen-bonded polymer blends at the air-water interface: poly(vinylacetate) + poly(4-hydroxystyrene). Colloid Polym Sci 1998;276:960–7.
[20] Monroy F, Ortega F, Rubbio RG. Rheology of a miscible polymer blend at the air-water interface. Quasielastic surface light scattering study and analysis in terms of staric and dynamic scaling laws. J Phys Chem B 1999;103:2061–71.
[21] Rivillon S, Monroy F, Ortega F, Rubio RG. Dilational rheology of monolayers of a miscible polymer blend. Eur Phys J E Soft Matter 2002;E9:375–85.
[22] Kawaguchi M, Suzuki M. Mixed films of poly(n-hexyl isocyanate) and poly(vinyl acetate) at the air-water interface. J Colloid Interface Sci 2005;288:548–52.
[23] Ohkita M, Higuchi M, Kawaguchi M. AFM studies on LB films of poly(n-hexyl isocyanate), poly(vinyl acetate), and their binary mixtures. J Colloid Interface Sci 2005;292:300–3.
[24] Morioka T, Kawaguchi M. Surface dilatational moduli of poly(vinyl acetate) (PVAc) and PVAc-poly(n-hexyl acetate) (PHIC) blend films at the air-water interface. Langmuir 2011;27:8672–7.
[25] Ito H, Russell TP, Wignall GD. Interactions in mixtures of poly(ethylene oxide) and poly(methyl methacrylate). Macromolecules 1987;20:2213–20.
[26] Hiles H, Monroy F, Bonales LJ, Ortega F, Rubio RG. Fourier-transform rheology of polymer Langmuir monolayers: analysis of the non-linear and plastic behaviors. Adv Colloid Interface Sci 2006;122:67–77.
[27] Higuera M, Peraies JN, Vega JM. The role of fluid dynamics on compression/expanded surfactant monolayers. Phys Fluids 2016;28:062108.
[28] Bykov AG, Liggieri L, Noskov BA, Pandolfini P, Ravera F, Loglio G. Surface dilational rheological properties in the nonlinear domain. Adv Colloid Interface Sci 2015;222:110–8.
[29] Chen S, Yoshioka T, Lucarelli M, Hwang LH, Langer R. Controlled delivery systems for proteins based on poly(lactic/glycolic acid) microspheres. Pharm Res 1991;8:713–20.
[30] Vert M, Schwach G, Engel R, Coudane J. Something new in the field of PLA/GA bioresorbable polymers? J Control Release 1998;53:85–92.
[31] Nagata K, Kawaguchi M. Ellipsometric study of binary mixed films of poly(ethylene oxide) and poly(methyl methacrylate) at the air/water interface. Macromolecules 1990;23:3957–62.
[32] Noskov BA. Dynamic surface elasticity of polymer solutions. Colloid Polym Sci 1995;273:263–70.
[33] Murakami H, Norisuye T, Fujita H. Dimensional and hydrodynamic properties of poly(hexyl isocyanate) in hexane. Macromolecules 1980;13:345–52.
[34] Kawaguchi M, Yamamoto M, Kurauchi N, Kato T. Surface pressure and fluorescence microscopy studies of poly(n-hexyl isocyanate) films spread at the air-water interface. Langmuir 1999;15:1388–91.
[35] Yoshida S. Surface dilational moduli of PEO/PVAc blend films spread at the air-water interface. Master's thesis at Mie University; 2014.
[36] Mitsui N, Morioka T, Kawaguchi M. Surface dilational moduli of poly(vinyl acetate), poly(methyl methacrylate), and their blend films spread at the air-water interface. Colloids Surf A Physicochem Eng Asp 2012;395:248–54.
[37] Kawaguchi M, Nishida R. Compatibility of polymer chains at the air/water interface. Langmuir 1990;6:492–6.
[38] Kawaguchi M, Nagata K. Ellipsometric study of mixture films of poly(methyl acrylate) and poly(vinyl acetate) at the air/water interface. Langmuir 1991;7:1478–82.
[39] Rung FE, Yu H. Thin films of a binary polymer systems: poly(vinyl acetate)/poly (dimethylsiloxane) layers at the air/water interface. Langmuir 1993;9:3191–9.
[40] Kawaguchi M, Suzuki S, Imae T, Kato T. Surface morphology of Langmuir-Blodgett blend films of poly(vinyl acetate)-poly(methyl acrylate). Langmuir 1997;13:3794–9.